J Forensic Sci, September 2009, Vol. 54, No. 5
doi: 10.1111/j.1556-4029.2009.01108.x
Available online at: www.blackwell-synergy.com

John W. Bond,[1,2] *D.Phil.*

Visualization of Latent Fingerprint Corrosion of Brass

ABSTRACT: Visualization of latent fingerprint deposits on metals by enhancing the fingerprint-induced corrosion is now an established technique. However, the corrosion mechanism itself is less well understood. Here, we describe the apparatus constructed to measure the spatial variation (ΔV) in applied potential (V) over the surface of brass disks corroded by latent fingerprint deposits. Measurement of ΔV for potential of 1400 V has enabled visualization of fingerprint ridges and characteristics in terms of this potential difference with ΔV typically of a few volts. This visualization is consistent with the formation of a Schottky barrier at the brass-corrosion product junction. Measurement of the work function of the corroded brass of up to 4.87 ± 0.03 eV supports previous results that suggested that the corrosion product is composed of p-type copper oxides. A model for the galvanic corrosion of brass by ionic salts present in fingerprint deposits is proposed that is consistent with these experimental results.

KEYWORDS: forensic science, latent fingerprint, print visualization, metal surface, electrochemical mechanism, latent fingerprint components

When latent fingerprints are deposited on metal surfaces such as brass, common enhancement techniques include powdering, vacuum metal deposition, and various chemical treatments, such as cyanoacrylate fuming, dyeing, and immersion in small particle suspensions (1). All of these techniques require some form of physical or chemical interaction between the enhancing reagent and the fingerprint deposit, the technique selected depending on the history of the item being treated, for example, whether it has been exposed to elevated temperatures, wetted, etc. (2).

Recent research has focussed on noninvasive fingerprint visualization techniques that do not compromise associative trace evidence that may be present in the fingerprint deposit. Crane et al. (3) have demonstrated how molecular absorption of infrared radiation by fatty acid esters present in the fingerprint deposit can be used to visualize latent fingerprints on a variety of surfaces including metals. The technique uses Fourier transform infrared spectroscopic imaging, first reported by Bartick et al. (4). Williams et al. (5) and Williams and McMurray (6) have demonstrated fingerprint visualization on a variety of metals using a Scanning Kelvin Microprobe. This technique is based on a measurement of the potential difference arising between a wire probe and the metal surface due to differences in their respective work functions (φ), the magnitude of this potential difference being affected by fingerprint deposits on the metal surface. Both techniques provide a spatial distribution of the measured parameter (reflected infrared energy or work function difference) and hence provide a noninvasive visualization of the fingerprint.

Williams et al. (5) considered the observed work function difference to be associated with the presence of ionic salts in the fingerprint deposit that acted as the electrolyte in an electrochemical reaction between the fingerprint deposit and the metal, resulting in galvanic corrosion to the metal surface. They reported that rubbing fingerprint deposits vigorously with a paper tissue several days after deposition had little effect on work function measurements which would support their fingerprint visualization resulting primarily from a reaction between the metal and fingerprint deposit.

This ability of latent fingerprint deposits to undergo a chemical reaction with metal substrates and thereby change the chemical properties of the metal surface has been known for many years (7). Recently, we have considered the corrosion of a range of metal elements and alloys by fingerprint deposits (8,9). We have shown how leaving fingerprint deposits on brass in air at room temperature for several days caused sufficient corrosion of the metal to enable the fingerprint to be visualized even after the residue of the fingerprint deposit had been removed by cleaning the metal in warm water to which a few drops of commercial detergent had been added. This visualization was achieved by employing a novel technique which required the application of a potential to the brass (>1 kV) followed by the introduction of a conducting carbon powder (grain size ~10 μm) (8). The introduction of the conducting powder was facilitated by using Cascade Developer (Foster and Freeman, Evesham, U.K.) which comprised ~400 μm spherical beads that were coated with the conducting powder. By rolling the spherical beads back and forth across the charged brass surface, the conducting powder was found to adhere preferentially to the areas of corrosion on the metal thus enabling the fingerprint to be visualized. The degree of enhancement of the fingerprint varied between brass samples and we postulated that this was due to both the variable composition of sweat in the fingerprint deposit and the amount of sweat secreted by individuals (10). In particular, in keeping with corrosion science (11) and the work of Williams et al. (5), we felt that the presence of aggressive ions (such as chloride) would enhance the corrosion of brass by the fingerprint deposit and possibly the degree to which the applied potential and conducting powder would enhance the visualization of the fingerprint. Subsequently, we have shown corroded parts of the brass to have a potential lower than that applied to the bulk, typically up to 12 V for an applied potential of 1400 V. Further, we have discovered that the junction between the bulk and corroded brass can exhibit the characteristics of a rectifying metal–semiconductor contact with

[1]Scientific Support Unit, Northamptonshire Police, Wootton Hall, Northampton NN4 0JQ, UK.
[2]Forensic Research Centre, University of Leicester, Leicester LE1 7EA, UK.

Received 22 July 2008; and in revised form 17 Sept. 2008; accepted 12 Oct. 2008.

the corroded brass exhibiting the properties of a p-type semiconductor, this semiconductor most likely being copper (I) or copper (II) oxide (12). This type of rectifying metal–semiconductor contact requires the work function of the metal (φ_{brass}) to be less than the semiconductor ($\varphi_{s\text{-}c}$) and is commonly known as a Schottky barrier (13–15). The work function of a solid (φ) is defined as the minimum energy required to remove an electron from the Fermi level energy of the solid (E_F) to the vacuum level energy. Figure 1*a* shows a schematic representation of an energy level diagram for a metal (metal "A") and a p-type semiconductor in which the work function of the metal (φ_{brass}) is less than the semiconductor ($\varphi_{s\text{-}c}$). As this is an energy level diagram, work functions are shown as energies (multiplied by q, the electronic charge) rather than as potentials. As $\varphi_{brass} < \varphi_{s\text{-}c}$, the Fermi level energy of the metal [$E_{F(brass)}$] is greater than the semiconductor [$E_{F(s\text{-}c)}$]. For the semiconductor, the electron valence band (E_v) and conduction band (E_c) energy levels are also shown. In Fig. 1*b*, the metal and semiconductor have been brought into contact resulting in electron flow from the metal to the semiconductor as $\varphi_{brass} < \varphi_{s\text{-}c}$. Electron flow continues until the Fermi levels in both materials are aligned and $E_{F(brass)} = E_{F(s\text{-}c)}$. The electric field generated by this electron flow acts to oppose further movement of charge, a situation known as thermal equilibrium. This electron flow and Fermi level alignment result in a bending of the semiconductor conduction and valence bands upwards as shown and a depletion of the concentration of majority carrier holes in the vicinity of the metal–semiconductor junction. This majority carrier depletion extends a distance W into the semiconductor as shown in Fig. 1*b*. The net result is the creation of a potential barrier (φ_b) that must be overcome by the majority carrier holes for a conduction current to flow between the metal and semiconductor. A positive or negative bias applied to the semiconductor (with respect to the metal) has the effect of either lowering or raising the potential barrier, thereby giving rise to a practical application of a Schottky barrier, namely, a Schottky barrier diode. Figure 1*c* shows a schematic representation of a Schottky barrier diode forward biased in an electrical circuit and formed with a Schottky barrier between a metal (metal "A") and a p-type semiconductor. Electrical contact is made to the other end of the semiconductor with a metal (metal "B") that has a work function greater than the semiconductor, thereby giving rise to an ohmic contact rather than a rectifying contact.

In this paper, we show how a measurement of the spatial distribution of the variation (ΔV) in applied potential (V) over the surface of planar brass disks, subject to corrosion by latent fingerprint deposits, can be used to visualize fingerprint ridge detail. We measure the spatial distribution of ΔV for brass disks exhibiting a range of visible corrosion and relate this to the measured work functions for both the bulk and corroded brass. We then propose a model for the corrosion of brass by fingerprint deposits that can account for the formation of a Schottky barrier and the experimental results obtained.

Materials

One mm thick, 50 mm diameter brass disks (67% copper and 33% zinc) were sourced from Nobles Engineering (Northampton, U.K.). Prior to any fingerprint deposition, all disks were washed in 0.5 L of warm water containing a few (three to four) drops of a commercial detergent (containing both anionic and nonionic surfactants). Following this, all samples were washed in distilled water, acetone, and then again in distilled water. Finally, each sample was dried with a paper towel. Fingerprints were deposited by pressing a finger onto the metal surface for 1–2 sec with a light pressure sufficient to ensure contact between the finger and metal. While no attempt was made to regulate the amount of pressure applied by individuals, this procedure was intended to produce reasonably uniform deposition. All fingerprint donors washed their hands with soap and water 20 min prior to depositing fingerprints and no artificial stimulation of sweat was employed such as placing the hand in a plastic bag (16) or wearing a latex glove prior to deposition (17).

Forty donors each provided one fingerprint deposit onto different brass disks, thus giving 40 brass disk samples in total. All samples were left in air at room temperature (18 ± 5°C) for a period of 5 days, this time period being the same as in our previous work (8). After the 5-day period, samples were washed in a 0.5 L solution of warm water containing a few drops of the commercial detergent used to initially clean the disks. The disks were rubbed vigorously with a nonabrasive cloth to remove all traces of fingerprint deposit.

Methods

Apparatus to measure the spatial distribution of ΔV over the surface of metal disks has been described previously (12) and is shown schematically in Fig. 2. A sample brass disk was positioned horizontally on to a brass plate and held securely by means of an insulating rigid polymer ring and clamp, the ring being machined to provide a clearance hole for the brass disk. The potential (V) was applied to the brass plate which was in good electrical contact with the sample disk. The probe to sample the potential at the corroded surface of the brass was made from a platinum rod ~0.5 mm diameter, formed into a tip at one end of ~10 μm diameter (Cripton Jewellers, Birmingham, U.K.). Such a diameter was deemed suitable for the measurements to be undertaken as fingerprint deposits on smooth nonporous surfaces have been measured at widths of up to ~100 μm (18), an order of magnitude bigger than the tip of the probe.

Between measurements, the probe was raised and lowered onto the surface of the sample brass disk by means of a slow acting solenoid (1 mm/sec) and the probe was supported by passing it through a vertical brass sleeve and machined to provide a clearance hole for the platinum probe. Contact between the probe and the sample disk was maintained by the weight of the probe itself. Scanning of the sample in both x and y directions was carried out using a micromanipulation stage consisting of two orthogonally arranged linear bearings (Del-Tron Precision Inc., Bethel, CT) placed on shock absorbers to prevent any mechanical disruption of the contact between the probe and the sample disk. Electrical output from the probe was taken via the brass sleeve.

Any difference (ΔV) between the potential applied to the sample brass disk (V) and the platinum probe was measured by means of a differential probe (Elditest, GE 8115, Sefram, St. Etienne, France) rated to a maximum differential and common mode input voltage of ±1500 V.

Platinum was selected for the probe to ensure an ohmic contact between the probe and the corroded brass and our previous work has shown that $\varphi_{brass} < \varphi_{s\text{-}c} < \varphi_{Pt,}$ where φ_{Pt} is the work function of platinum (12). For a p-type semiconductor, an ohmic contact was obtained at a metal junction when the semiconductor had a lower work function than the metal, that is, $\varphi_{s\text{-}c} < \varphi_{Pt}$. The performance of this apparatus has been tested previously by measuring ΔV against V for a variety of known ohmic resistances (12).

Results

Potential difference for the 40 brass disks subject to the deposition of fingerprints and subsequent washing as described above was

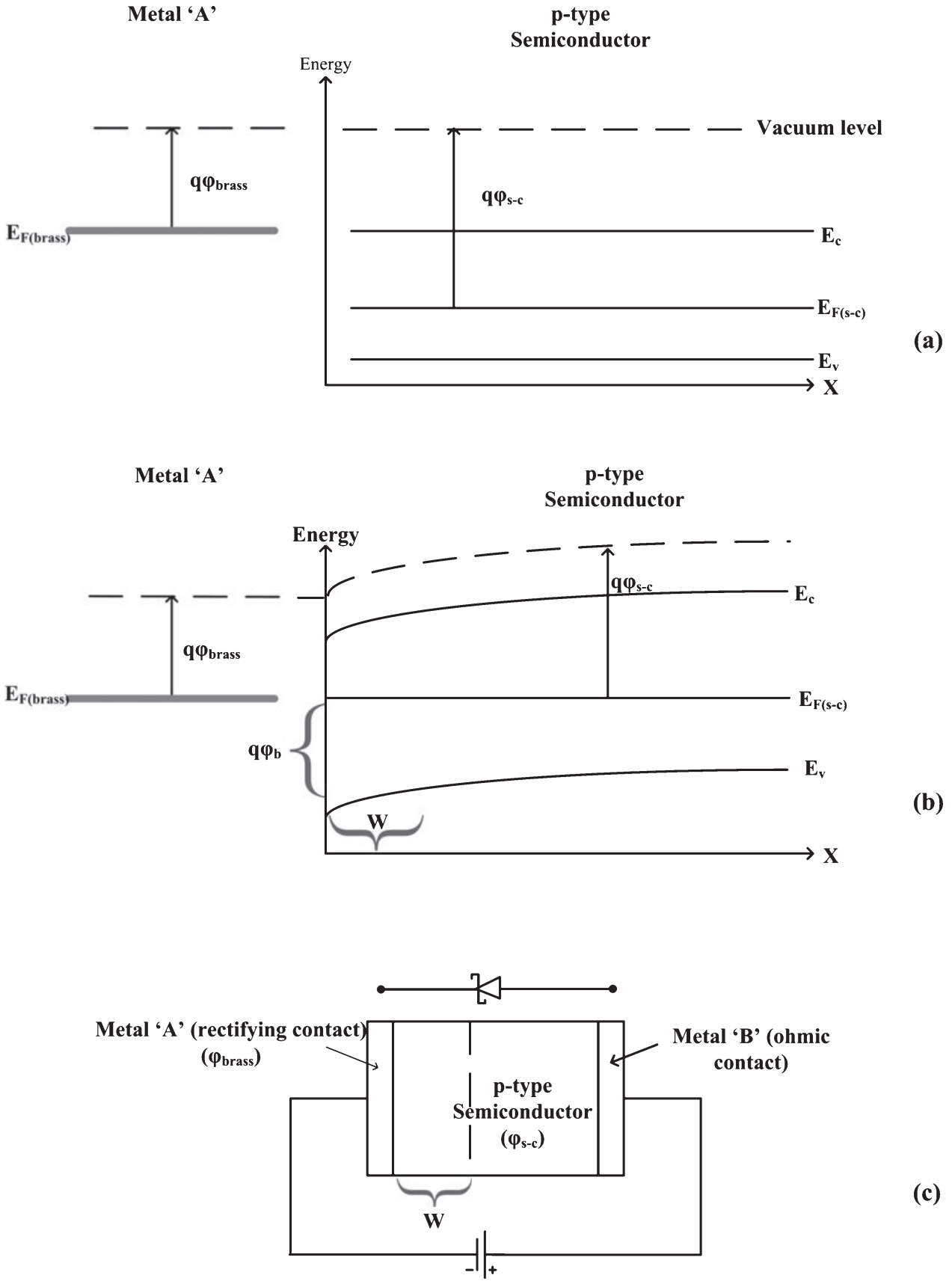

FIG. 1—*Schematic representation of the energy level diagram for a metal and p-type semiconductor in which the work function of the metal is less than the work function of the semiconductor. (a) shows that two materials are separated and (b) in contact with a resulting bending of the semiconductor energy bands. W represents the width of the majority carrier depletion in the semiconductor and* $q\varphi_b$*, the energy of the potential barrier. (c) shows a schematic representation of a Schottky barrier diode formed from a metal and p-type semiconductor and forward biased.*

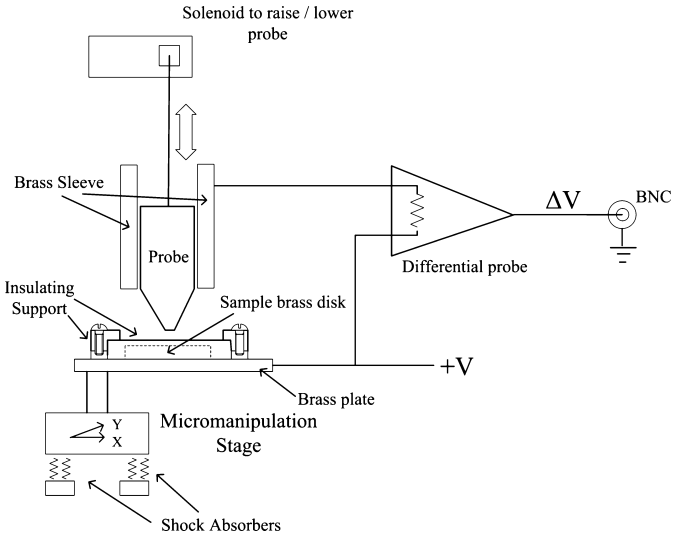

FIG. 2—*Schematic diagram illustrating apparatus constructed to measure the spatial distribution of ΔV across the surface of a sample brass disk. BNC, Bayonet Neill-Concelman*

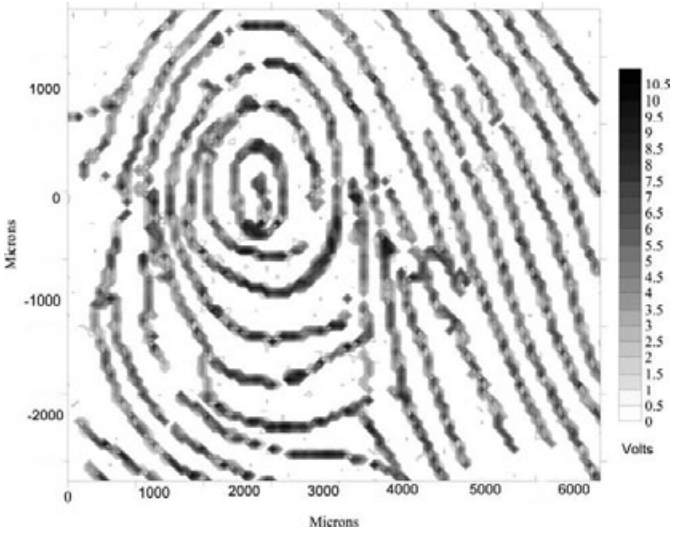

FIG. 3—*Grayscale contour image of spatial distribution of −V for disk A measured at intervals of 25 μm. The peak value of ΔV is ∼10.5 V*

measured using the apparatus shown in Fig. 2 with a potential of 1400 V. This value for V was selected as it was less than the operating limit of the differential probe. Each scan was carried out across the surface of the disk at 25 μm intervals through an area in which the fingerprint was deposited. Twenty-five μm intervals were chosen as this was greater than the diameter of the tip of the probe and less than the anticipated width of any corrosion caused by the fingerprint deposit (18). Of the 40 brass disks only 11 showed any coherent variation in potential across the surface of the disk. By coherent we mean linear distances where $\Delta V > 0.5$ V for at least three consecutive measurement intervals (a distance of 50 μm). Spatial variation >0.5 V was above the limit of detection of the apparatus of ∼0.3 V (based on the quoted output noise level of the differential probe and what, in practice, could be measured). These 11 disks also exhibited the presence of a Schottky barrier between the bulk and corroded brass, the determination of which has been described previously (12).

Of the 11 disks that gave a coherent ΔV, a typical example of the spatial distribution of ΔV for full ridge detail visualization is shown in Fig. 3 (referred to as disk A) as a grayscale contour image generated from cartography software (Golden Software Inc., Golden, CO). The peak value of ΔV in Fig. 3 was measured at ∼10.5 V. The average work function of areas of corroded brass ($\varphi_{s\text{-}c}$) was measured by a Scanning Kelvin Probe for disk A at 4.86 ± 0.03 eV (KP Technology, Wick, U.K.).

For comparison, an inked impression of the same finger is shown in Fig. 4. Although parts of some of the ridge lines evident in the inked impression were absent from the spatial distribution of ΔV, generally the ridge characteristics were represented well in the ΔV scan, which displayed consistent values for ΔV across the corroded area of the disk.

The absence of parts of ridge lines in Fig. 3 is most likely due to an absence of corrosion at these points on the disk. Also, the width of each ridge in Fig. 3 appears less than the inked impression, suggesting that the corrosion does not extend over the full width of the impressed fingerprint on the brass. For comparison, a wire frame image of the spatial distribution of ΔV for disk A is shown in Fig. 5, which is also generated from the cartography software.

FIG. 4—*Inked impression of the fingerprint from disk A shown in Fig. 3.*

The disk shown in Fig. 3 displays little visible corrosion and is therefore enhanced by applying a potential and conducting powder to the disk as described above (8). The result of this enhancement is shown in Fig. 6 along with a photograph of the corroded disk after washing and prior to enhancement.

Other disks that gave coherent ΔV displayed varying degrees of visible corrosion. Figure 7 shows the corrosion on a disk (referred to as disk B) that required no enhancement to aid visualization after washing. Application of a potential and conducting powder did result in powder adhering to the areas of corrosion, although little improvement in visualization was obtained.

Figure 7 shows clearly the corrosion on this disk to be made up of a series of dots along the ridge lines. Such fingerprint images are well known (18) and are indicative of sweat secretion from papillary ridge pores that is insufficient to form continuous lines of ridges, forming instead "pools" of deposit around the pores (19). The white box in Fig. 7 shows the approximate area of the spatial distribution of ΔV recorded for disk B, which is shown in Fig. 8 with the peak value of ΔV being ∼7 V, lower than ΔV for Fig. 3. However, the average work function of the corroded brass ($\varphi_{s\text{-}c}$)

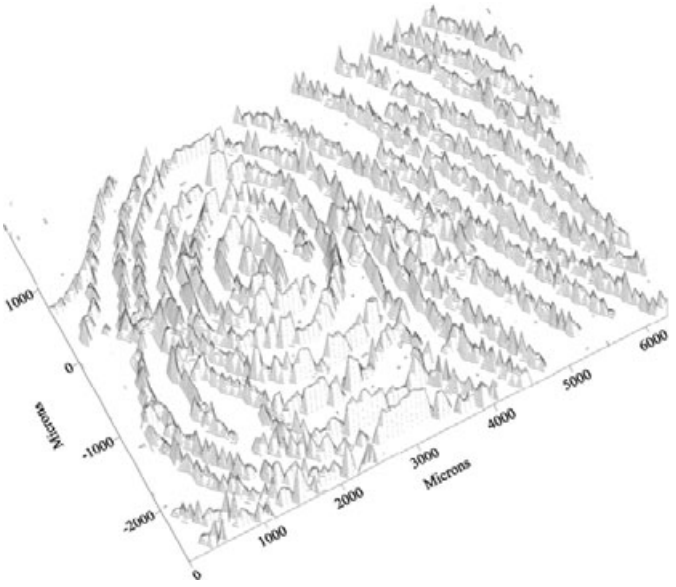

FIG. 5—*Grayscale wire frame image of spatial distribution of −V for disk A measured at intervals of 25 μm. The peak value of ΔV is ∼10.5 V.*

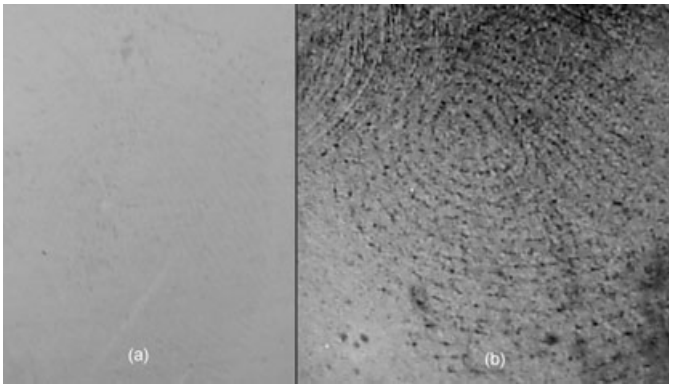

FIG. 6—*Fingerprint corrosion on brass disk A after washing and (a) before and (b) after the application of a potential and conducting powder.*

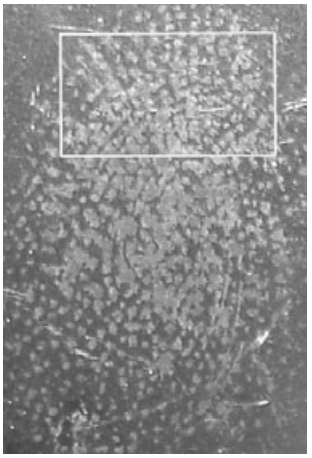

FIG. 7—*Fingerprint corrosion on brass disk (disk B) that gave a peak value of ΔV of ∼7 V. The white box shows the approximate area of the spatial distribution of ΔV shown in Fig. 8.*

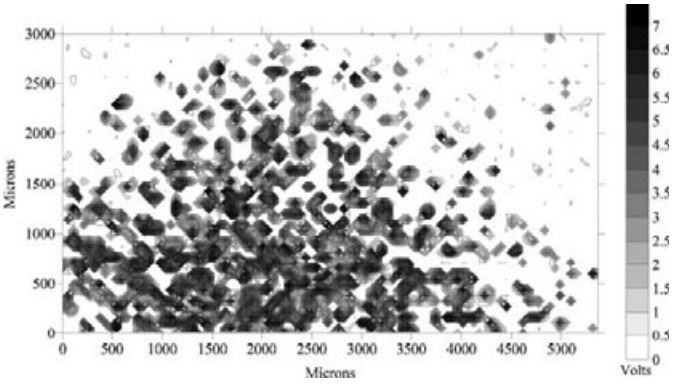

FIG. 8—*Grayscale contour image of spatial distribution of ΔV for disk B measured at intervals of 25 μm. The peak value of ΔV is ∼7 V.*

was measured at 4.87 ± 0.03 eV, which was the same as disk A within the error limit of the measurement.

Disks that gave no coherent ΔV ranged from displaying no visible corrosion after washing to full ridge detail development, which was consistent with our previous experiments (8). None of these disks produced any improvement in ridge detail visualization following the application of a potential and conducting powder and none exhibited the presence of a Schottky barrier. An example of a disk displaying full ridge development is shown in Fig. 9 (referred to as disk C). This disk gave an average corroded brass work function measurement ($\varphi_{s\text{-}c}$) of 4.79 ± 0.01 eV less than $\varphi_{s\text{-}c}$ for disks A and B, and within the error limit of the measurements same as the measured value for the bulk brass (φ_{brass}) of 4.77 ± 0.02 eV.

Figure 9 shows clearly the clarity of the corroded impression including third level fingerprint characteristics such as pore location or poroscopy (20). We have found this clarity previously on other metal alloys containing a high percentage of copper (9).

FIG. 9—*Fingerprint corrosion on brass disk (disk C) that gave no coherent ΔV and did not exhibit the characteristics of a Schottky barrier.*

Discussion

We now relate these results to the model for the galvanic corrosion of metal by fingerprint deposits proposed by Williams et al. (5,6) and in our previous work (8,12). In this model, both electrodes (anode and cathode) are formed on the metal surface beneath the fingerprint deposit and the electrical circuit is completed by electron flow through the metal. Such an electrochemical cell obeys mixed-potential theory and consists of both oxidation and reduction half-cell reactions with no net accumulation of charge, that is, the rate of oxidation equals the rate of reduction (21).

First, we consider the scenario where there is little or no ionic salt present in the fingerprint deposit which, for an eccrine deposit, would therefore consist mainly of water (10). If thermodynamically favorable, each fingerprint ridge in the deposit gives rise to a differential aeration corrosion cell, so called because of the time-dependent spatial variation of oxygen in the cell (22). Figure 10*a* shows a schematic representation of a cross-section through a corrosion cell formed from a ridge in the fingerprint deposit, immediately after deposition, onto a metal M.

The cathodic reaction for such a cell (22) is given by

$$O_2 + 2H_2O + 4e^- \rightleftharpoons 4OH^- \qquad E^0 = 0.4\text{eV} \qquad (1)$$

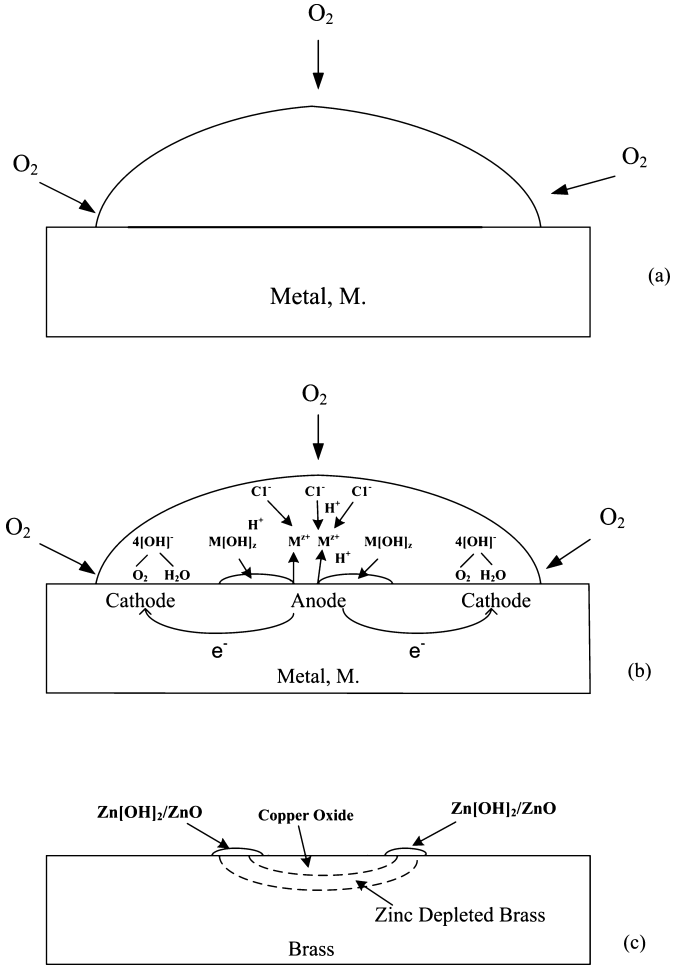

FIG. 10—*Schematic representation of a section through a fingerprint ridge deposit onto the surface of a metal M. (a) shows the deposit immediately after deposition, (b) shows the corrosion reaction enhanced by the presence of chloride ions, (c) shows the layers of corrosion product after completion of the corrosion process.*

where E^0 is the standard reduction potential of the half-cell reaction shown (21,23). The general half-cell anodic reaction for metal *M* is (22)

$$M \rightleftharpoons M^{z+} + ze^- \qquad (2)$$

For the reaction to be thermodynamically favorable the cell potential which is the sum of the oxidation potential of the anode and the reduction potential of the cathode must be >0 (9,21). For brass

$$Zn \rightleftharpoons Zn^{2+} + 2e^- \qquad (3)$$

$$Cu \rightleftharpoons Cu^{2+} + 2e^- \qquad (4)$$

and

$$Cu^{2+} + e^- \rightleftharpoons Cu^+ \qquad (5)$$

are thermodynamically favorable (11).

Initially, these reactions (Eqs [1] and [2]) can occur over the whole brass surface that is covered by ridges of the deposit (21), leading to the formation of metal hydroxides that tend to passivate the surface of the brass (11,24). This is a scenario consistent with the results for disk C in that a uniform discoloration of the metal occurred coincident with the lines of ridges of the fingerprint. As zinc is more electropositive than copper (a lower value of E^0), it might be expected that the passivating layer produced would consist mainly of zinc hydroxide or dehydrated as zinc oxide. However, the corroded brass work function measurement ($\varphi_{s\text{-}c}$) for disk C of 4.79 ± 0.01 eV was greater than measured values for a thin film of zinc oxide of 4.47 eV (25) and was consistent with the measured value for the bulk brass of 4.77 ± 0.02 eV. Therefore, it may be that a combination of metal hydroxides and oxides is produced, contributing to the overall measured work function of the corroded brass. As disk C did not produce either a Schottky barrier or coherent ΔV, clearly, a more complex reaction was required between the fingerprint deposit and brass in order for these to occur.

Consider now the scenario in which the fingerprint deposit is rich in ionic salts. The above model holds until the cathodic reaction (Eq. [1]) leads to an oxygen concentration gradient in the ridges of the deposit as oxygen from the air diffuses into the edge of the ridges more readily than into the center. Eventually, the center of each ridge deposit can no longer support the reaction of Eq. (1) and the cathodic reaction moves to the periphery of the ridge deposits, separating the anode and cathode, with an anode forming at the oxygen-depleted center of the ridge deposit. To prevent an accumulation of charge and to obey mixed-potential theory (21), the smaller surface area of the anode (with respect to the cathode) increases the positive current density at the anode which attracts negative ions from the ionic salts (such as chloride) forming a metal chloride of the general form

$$M^{z+} + zCl^- \rightleftharpoons MCl_z \qquad (6)$$

As the ionic salts are secreted from ridge pores in the center of each ridge, the chloride ions will also have a concentration gradient with the highest concentration, initially, at the center of the ridge deposit, coincident with the anode. Thus, the chloride ions are concentrated in the correct location to be attracted to the metal ions. This formation of the anode at the center of each ridge deposit may explain why the width of each corrosion ridge in Fig. 3 appears less than the inked impression, Fig. 4.

Hydrolysis of the metal chloride by water present in the fingerprint ridge deposit gives

$$MCl_z + zH_2O \rightleftharpoons M(OH)z + zHCl \quad (7)$$

$$HCl \rightleftharpoons H^+ + Cl^- \quad (8)$$

The formation of hydrochloric acid has the effect of reducing the pH at the anode and increasing the rate of reaction of Eq. (2) (23). A schematic representation of this is shown in Fig. 10*b*.

Clearly, this reaction will be limited by the availability of the solution (the water from the fingerprint deposit) to transport the electrolyte which will evaporate eventually stopping the movement of ions and hence the corrosion process. The concentration of ions within the solution will increase as the solution evaporates and this will affect the transport process of the ions (26).

We now suggest this removal of metal ions through the presence of ionic salts as an explanation for the formation of the Schottky barrier. It is well known that brass composed of 15% or more zinc is subject to the selective leaching of zinc from the brass (dezincification), this increasing as the percentage of zinc increases (24) and as the concentration of chloride ions increases (11) as zinc is more electropositive than copper. Thus, it would be reasonable to expect a fingerprint deposit rich in ionic salts to leach zinc from the brass leaving a layer of zinc-depleted brass (i.e., copper) that was available for oxidation via the hydroxyl ions (OH^-) produced at the cathode with copper (II) hydroxide dehydrating readily to form black copper (II) oxide (27). This would result in the formation of a layer of p-type copper oxide above a layer of zinc-depleted brass that, itself, would lie above the bulk brass. Pchelnikov et al. (28) have shown that when brass is immersed in a sodium chloride solution, zinc is initially dissolved preferentially into solution followed by the dissolution of both zinc and copper. Pchelnikov et al. found that above a certain concentration of copper ions in solution, the copper redeposited onto the metal surface producing a copper-enriched layer. Figure 10*c* shows these layers schematically with the leached zinc precipitating as zinc hydroxide or dehydrated as zinc oxide in the area around the anode in accordance with Eq. (7). In this model, the Schottky barrier would comprise of a zinc-depleted brass–copper oxide junction.

Measurements of $\varphi_{s\text{-}c}$ for disks A and B of 4.86 ± 0.03 and 4.87 ± 0.03 eV, respectively, are consistent with the corroded brass being composed of copper oxides as both copper (I) and copper (II) oxide behave as p-type semiconductors (29) and have measured work functions of ~4.76 eV [copper (I) oxide] and ~5.3 eV [copper (II) oxide] (30). The measured value for n-type zinc oxide was lower at 4.47 eV (25).

Dissolution of metal in the presence of fingerprint deposits has also been observed in relation to the gripping of firearms. Avissar et al. (31) noted that components of sweat such as chloride ions influenced the degree of iron oxide dissolution from firearms onto the hand when gripped with a moistened (sweat rich) hand. While Avissar et al. did not discuss the mechanism for this dissolution, galvanic corrosion similar to that described here is likely.

This model requires the presence of ionic salts in fingerprint deposits and further work is in hand to correlate the composition of eccrine sweat with the formation of a Schottky barrier to test the validity of the model. Quantification of the characteristics of the Schottky barrier is also being undertaken.

We have commented previously on the relative ease with which fingerprint corrosion of brass can form a rectifying metal–semiconductor contact (12) and the model proposed here for the corrosion of brass and oxide formation is not dissimilar to methods employed in the manufacturer of commercial Schottky barrier diodes such as electrochemical anodization (14).

Acknowledgments

The author is indebted to the many members of Northamptonshire Police who willingly donated their latent fingerprints for this research. The assistance of Mrs. Trudy Loe (Research Assistant Northamptonshire Police) with the preparation of the manuscript is acknowledged. The support from the Chief Officers of Northamptonshire Police to conduct this research is gratefully acknowledged.

References

1. Bowman V, editor. Manual of fingerprint development techniques, 2nd rev ed. Sandridge, U.K.: Police Scientific Development Branch, Home Office, 2004.
2. Lee HC, Gaensslen RE. Methods of latent fingerprint development. In: Lee HC, Gaensslen RE, editors. Advances in fingerprint technology. New York: Elsevier, 2001;105–75.
3. Crane NJ, Bartick EG, Perlman RS, Huffman S. Infrared spectroscopic imaging for non-invasive detection of latent fingerprints. J Forensic Sci 2007;52:48–53.
4. Bartick E, Schwartz R, Bhargava R, Schaeberle M, Fernandez D, Levin I. Spectrochemical analysis and hyperspectral imaging of latent fingerprints. In: Baccino E, editor. Proceedings of the 16th Meeting of the International Association of Forensic Sciences, Montpellier, France, 2–7 September, 2002. Bologna, Italy: Monduzzi Editore, IPD, 2002:61–4.
5. Williams G, McMurray HN, Worsley DA. Latent fingerprint detection using a scanning Kelvin microprobe. J Forensic Sci 2001;46:1085–92.
6. Williams G, McMurray N. Latent fingermark visualization using a scanning Kelvin probe. Forensic Sci Int 2007;167:102–9.
7. Pascoe MW, Richardson MOW. A new method for the detection of thin films on steel. Wear 1971;18:76–78.
8. Bond JW. Visualization of latent fingerprint corrosion of metallic surfaces. J Forensic Sci 2008;53:812–22.
9. Bond JW The thermodynamics of latent fingerprint corrosion of metal elements and alloys. J Forensic Sci 2008;53:doi: 10.1111/j.1556-4029.2008.00860.x.
10. Ramotowski RS. Composition of latent finger print residue. In: Lee HC, Gaensslen RE, editors. Advances in fingerprint technology. New York: Elsevier, 2001;63–104.
11. Trethewey KR, Chamberlain J. Corrosion for science and engineering. Harlow, England: Longman Scientific, 1995;336–426.
12. Bond JW On the electrical characteristics of latent finger mark corrosion of brass. J Phys D Appl Phys 2008; doi: 10.1088/0022-3727/41/12/125502.
13. Bar-Lev A. Semiconductors and electronic devices. Hemel Hempstead: Prentice Hall, 1993;96–124.
14. Sze SM. Semiconductor devices. Danvers: Wiley, 2002.
15. Fraser DA. The physics of semiconductor devices. New York: Oxford University Press, 1986;132–63.
16. Migron Y, Hocherman G, Springer E, Almog J, Mandler D. Visualization of sebaceous fingerprints on fired cartridge cases: a laboratory study. J Forensic Sci 1998;43:543–8.
17. Worley CG, Wiltshire SS, Miller TC, Havrilla GJ, Majidi V. Detection of visible and latent fingerprints using micro-x-ray fluorescence elemental imaging. J Forensic Sci 2006;51:57–63.
18. Thomas GL. The physics of fingerprints and their detection. J Phys E Sci Instrum 1978;11:722–31.
19. Leggett R, Lee-Smith EE, Jickells SM, Russell DA. "Intelligent" fingerprinting: simultaneous identification of drug metabolites and individuals by using antibody-functionalized nanoparticles. Angew Chem Int Ed 2007;46:4100–3.
20. Ashbaugh DR. Quantitative-qualitative friction ridge analysis. Boca Raton: CRC Press, 1999.
21. Trethewey KR, Chamberlain J. Corrosion for science and engineering. Harlow, England: Longman Scientific, 1995;69–190.

22. Mattsson E. Basic corrosion technology for scientists and engineers. Wandsworth, England: Institute of Materials, 2001;135–80.
23. Landolt D. Corrosion and surface chemistry of metals. Lausanne, Switzerland: CRC Press, 2007;15–58.
24. Landolt D. Corrosion and surface chemistry of metals. Lausanne, Switzerland: CRC Press, 2007;227–329.
25. Sundaram KB, Khan A. Work function determination of zinc oxide films. J Vac Sci Technol A 1997;15:428–30.
26. Bockris JO'M, Reddy AKN. Modern electrochemistry. New York: Plenum Press, 1998;361–599.
27. Housecroft CE, Sharpe AG. Inorganic chemistry. Harlow, England: Pearson, 2005;593–644.
28. Pchelnikov AP, Sitnikov AD, Marshakov IK, Losev VV. A study of the kinetics and mechanism of brass dezincification by radiotracer and electrochemical methods. Electrochimica Acta 1981;26:591–600.
29. Berger LI. Semiconductor materials. New York: CRC Press, 1997;295–409.
30. Assimos JA, Trivich D. The photoelectric threshold, work function, and surface barrier potential of single-crystal cuprous oxide. Phys Stat Sol (a) 1974;26:477–88.
31. Avissar YY, Sagiv AE, Mandler D, Almog J. Identification of firearms holders by the $[Fe(PDT)_3]^{+2}$ complex. Quantitative determination of iron transfer to the hand and its dependence on palmar moisture levels. J Forensic Sci 2004;49:1–5.

Additional information and reprint requests:
John W. Bond, D.Phil.
Scientific Support Unit
Northamptonshire Police
Wootton Hall
Northampton NN4 OJQ
United Kingdom
E-mail: john.bond@northants.police.uk